



**HAL**  
open science

## Water molecular state in 1-hexylpyridinium hexafluorophosphate: Water mean cluster size as a function of water concentration

Abdellatif Dahi, Kateryna Fatyeyeva, Corinne Chappey, Dominique Langevin, Stéphane Marais

► **To cite this version:**

Abdellatif Dahi, Kateryna Fatyeyeva, Corinne Chappey, Dominique Langevin, Stéphane Marais. Water molecular state in 1-hexylpyridinium hexafluorophosphate: Water mean cluster size as a function of water concentration. *Journal of Molecular Liquids*, 2019, 292, pp.111109. 10.1016/j.molliq.2019.111109 . hal-02329860

**HAL Id: hal-02329860**

<https://hal.science/hal-02329860v1>

Submitted on 25 Oct 2021

**HAL** is a multi-disciplinary open access archive for the deposit and dissemination of scientific research documents, whether they are published or not. The documents may come from teaching and research institutions in France or abroad, or from public or private research centers.

L'archive ouverte pluridisciplinaire **HAL**, est destinée au dépôt et à la diffusion de documents scientifiques de niveau recherche, publiés ou non, émanant des établissements d'enseignement et de recherche français ou étrangers, des laboratoires publics ou privés.



Distributed under a Creative Commons Attribution - NonCommercial 4.0 International License

# Water molecular state in 1-hexylpyridinium hexafluorophosphate: water mean cluster size as a function of water concentration

Abdellatif Dahi, Kateryna Fatyeyeva\*, Corinne Chappey, Dominique Langevin,  
Stéphane Marais

Normandie Univ., UNIROUEN, INSA ROUEN, CNRS, PBS, 76000 Rouen, France

\*Corresponding author: [kateryna.fatyeyeva@univ-rouen.fr](mailto:kateryna.fatyeyeva@univ-rouen.fr)

## Abstract

The water sorption behavior of representative pyridinium-based ionic liquid (IL), 1-hexylpyridinium hexafluorophosphate ([C<sub>6</sub>Py][PF<sub>6</sub>]), was studied over the whole range of the water activity  $a$  using a continuous gravimetric method. The analysis of the water sorption isotherm using the combination of a two-mode sorption (i.e. Henry-clustering) allowed to better understand [C<sub>6</sub>Py][PF<sub>6</sub>]-water interactions. At low and intermediate activity ( $a \leq 0.8$ ), the water molecules revealed a very low affinity to [C<sub>6</sub>Py][PF<sub>6</sub>] and, consequently, the water uptake was rather low. On the contrary, at high water activity ( $a > 0.8$ ), the water uptake increased exponentially and the water clustering easily occurred. The constant of the Henry-clustering equation as well as the water clustering mechanism in [C<sub>6</sub>Py][PF<sub>6</sub>] were discussed and compared to those of imidazolium-based ILs: 1-hexyl-3-methylimidazolium hexafluorophosphate [C<sub>6</sub>C<sub>1</sub>im][PF<sub>6</sub>] (water-immiscible IL) and 1-butyl-3-methylimidazolium tetrafluoroborate [C<sub>4</sub>C<sub>1</sub>im][BF<sub>4</sub>] (water-miscible IL). It is shown that the sorption of water molecules by pyridinium-based ILs is controlled not only by the anion's nature, but also by the cation's nature. Moreover, the Zimm-Lundberg theory was used to determine the water mean cluster size (MCS) in [C<sub>6</sub>Py][PF<sub>6</sub>], [C<sub>6</sub>C<sub>1</sub>im][PF<sub>6</sub>] and [C<sub>4</sub>C<sub>1</sub>im][BF<sub>4</sub>]. The MCS results confirmed the strong capacity of water molecules to be aggregated in [C<sub>6</sub>Py][PF<sub>6</sub>]. In order to have a deeper insight into the water molecular state, infrared spectroscopy measurements were carried out as a function of the relative humidity value and the obtained results were correlated with the results of water sorption isotherms. It is found that at high water activity ( $a > 0.8$ ), sorbed water molecules are strongly linked with ILs by hydrogen bonds and, therefore, are easily aggregated.

**Keywords:** room temperature ionic liquids, pyridinium-based cations, water sorption, mean cluster size, water molecular state.

## 34 **Introduction**

35

36 Room-temperature ionic liquids (RTILs) are becoming an interesting class of solvents  
37 for different applications. They possess attractive chemical and physical properties, and  
38 present several advantages compared to conventional solvents, such as good chemical and  
39 thermal stability, low volatility, non-flammability, and excellent and adjustable solvent  
40 properties<sup>1-4</sup>.

41 The most intensively studied class of RTILs is imidazolium-based RTILs.  
42 Nevertheless, pyridinium-based RTILs progressively attract attention recently. De los Rios *et al.*  
43 studied the use of alkylpyridinium-based cations combined with various anions as reaction  
44 media for the direct transesterification of sunflower-seed oil with methanol<sup>5</sup>. Padró *et al.*  
45 studied the partition coefficients of several compounds, some of them of biological and  
46 pharmacological interest, between water and RTILs based on the imidazolium, pyridinium,  
47 and phosphonium cations<sup>6</sup>. Zhang *et al.* showed that uranium formed various complexes with  
48 imidazolium- and pyridinium-based RTILs<sup>7</sup>. They came to conclusion that these RTILs might  
49 not only be useful in the extraction of uranium, but also showed high potential in the  
50 bioremediation of uranium waste stream. Behar *et al.* showed that the pulse radiolysis in  
51 alkylpyridinium-based RTILs allowed the production of a variety of radicals and the  
52 measurement of absolute rate constants of the reduction and oxidation of different molecules<sup>8</sup>.  
53 Siyuthin *et al.* showed that RTILs containing pyridinium cations and [PF<sub>6</sub>] anion efficiently  
54 catalyzed the asymmetric aldol reaction between aldehydes and ketones in the presence of  
55 water to generate aldols with high distereo- and enantio-selectivity<sup>9</sup>. Abdolmohammad-Zadeh  
56 *et al.* used 1-hexylpyridinium hexafluorophosphate ([C<sub>6</sub>Py][PF<sub>6</sub>]) for chemical modification  
57 of silica by means of the acid-catalyzed sol-gel processing<sup>10</sup>. The obtained RTIL-modified  
58 silica was employed as a solid phase extraction sorbent for removal of trace quantity of Fe(III)  
59 ions from aqueous samples. [C<sub>6</sub>Py][PF<sub>6</sub>] was also used as an extractant solvent in the  
60 preconcentration of trace quantity of zinc before its determination by flame atomic absorption  
61 spectrometry<sup>11</sup>. The combination of [C<sub>6</sub>Py][PF<sub>6</sub>]-based dispersive liquid-liquid micro-  
62 extraction (RTIL-based DLLME) with stopped-flow spectrofluorometry was applied to  
63 evaluate the concentration of aluminum Al(III) in different real samples at trace level<sup>12</sup>. Zeeb  
64 and Sadeghi proposed an efficient sample preparation method based on the application of  
65 [C<sub>6</sub>Py][PF<sub>6</sub>] as a microextraction solvent to preconcentrate and determine the trace quantity of  
66 Terazosin (a selective alpha-1 antagonist used for treatment of symptoms of an enlarged  
67 prostate)<sup>13</sup>.

68           However, in all these studies, the water behavior of pyridinium-based RTILs was not  
69 investigated, while it is known that the presence of water molecules is important for the  
70 separation or extraction capacities of these solvents. [C<sub>6</sub>Py][PF<sub>6</sub>], an example of RTIL highly-  
71 cited in the above studies, was just qualified as hydrophobic RTIL. But it is known that the  
72 majority of RTILs is hygroscopic and can absorb water from ambient air despite their  
73 hydrophobic character<sup>14-17</sup>. Their hygroscopic capacity depends mainly on the nature of their  
74 ions (cation and anion), the relative humidity and the temperature. In addition, it is established  
75 that the physical and chemical properties of RTILs are very sensitive to water content<sup>14-20</sup>.  
76 Therefore, it is essential to evaluate the possible interactions between water and pyridinium-  
77 based RTILs in order to estimate the real potential of this family of RTILs.

78           Numerous studies have already examined the solubility of pyridinium-based RTILs in  
79 water. For example, Neves *et al.* determined the solubility of 1-methyl-3-propylimidazolium  
80 and 1-methyl-3-propylpyridinium cations combined with the [PF<sub>6</sub>] anion in the temperature  
81 range from 288.15 to 318.15 K<sup>21</sup>. Freire *et al.* measured the solubility of imidazolium-,  
82 pyridinium-, pyrrolidinium-, and piperidinium-based RTILs in combination with different  
83 anions (bis-(trifluoromethylsulfonyl)imide, hexafluorophosphate, and tricyanomethane) in  
84 water between 288.15 and 318.15 K<sup>22</sup>. Yang *et al.* studied the solubility of 1-ethylpyridinium  
85 hexafluorophosphate in ethanol/water binary solvent mixture from 278.15 to 345.15 K<sup>23</sup>.  
86 Papaiconomou *et al.* studied the water solubility of RTILs containing 1-octylpyridinium, 1-  
87 octyl-2-methylpyridinium, or 1-octyl-4-methylpyridinium cations with various anions in two  
88 different experimental conditions, namely in equilibrium with the air and in the liquid water<sup>24</sup>.  
89 The solvatochromic solvent parameters of different RTILs based on imidazolium,  
90 hydroxyammonium, pyridinium and phosphonium cations at 298K using UV-Vis  
91 spectroscopy were studied<sup>25</sup>. However, to the best of our knowledge, no attempt has been  
92 made to quantify the possible interactions of water molecules and pyridinium-based RTILs in  
93 terms of both the water uptake and water behavior over the whole range of water activity.

94           The main objective of this work is to obtain a deeper understanding of the water  
95 sorption behavior of representative pyridinium-based RTIL, [C<sub>6</sub>Py][PF<sub>6</sub>], over the whole  
96 range of water activity. The choice of this IL is explained by the fact that this RTIL is among  
97 the most commonly used pyridinium-based RTILs in different fields of science. The  
98 measurements of water vapor sorption kinetics were carried out using the gravimetric method.  
99 The obtained water sorption isotherm was analyzed by using a two-mode sorption (Henry-  
100 clustering) in order to describe the water sorption behavior in [C<sub>6</sub>Py][PF<sub>6</sub>]. This model is  
101 based on the dual-model sorption idea, in which an ordinary dissolution (absorption)

102 described by Henry's law is combined with a clustering (aggregation) phenomenon. Water  
103 clustering involves multiple self-associated water molecules inside materials and it occurs  
104 mainly at high water activity. This model is the most appropriate as in this case the clustering  
105 phenomenon may be fitted separately from the Henry's linear part. The difference between  
106 the water sorption behavior of [C<sub>6</sub>Py][PF<sub>6</sub>] and imidazolium-based RTILs, 1-hexyl-3-  
107 methylimidazolium hexafluorophosphate ([C<sub>6</sub>C<sub>1</sub>im][PF<sub>6</sub>], water-immiscible RTIL) and 1-  
108 butyl-3-methylimidazolium tetrafluoroborate ([C<sub>4</sub>C<sub>1</sub>im][BF<sub>4</sub>], water-miscible RTIL), was  
109 discussed. The application of the Zimm-Lundberg theory to water sorption isotherm results  
110 made it possible to determine the mean cluster size (MCS) of water molecules in [C<sub>6</sub>Py][PF<sub>6</sub>],  
111 [C<sub>6</sub>C<sub>1</sub>im][PF<sub>6</sub>] and [C<sub>4</sub>C<sub>1</sub>im][BF<sub>4</sub>] as a function of the water concentration (or relative  
112 humidity). The infrared spectroscopy is extensively used for understanding the interactions  
113 between the water molecules and RTILs<sup>14</sup>. Therefore, the results of the water sorption were  
114 compared with the infrared spectroscopy results in order to discuss in details the molecular  
115 state of water molecules in RTILs.

116

## 117 **Experimental**

### 118 1) Materials

119 The chemical structure of RTILs used in this work, i.e. [C<sub>6</sub>Py][PF<sub>6</sub>], [C<sub>6</sub>C<sub>1</sub>im][PF<sub>6</sub>],  
120 and [C<sub>4</sub>C<sub>1</sub>im][BF<sub>4</sub>], is shown in Fig. 1. All RTILs were purchased from Acros Organics (>  
121 99% purity) in liquid state and used as received. All water used was Milli-Q water (18.2  
122 MΩ/cm at 25 °C, Millipore®). N<sub>2</sub> (99.99% purity, Air Products®) was used as received.

### 123 2) Sorption studies

124 The water vapor sorption kinetics measurements were carried out using a continuous  
125 gravimetric method. The electronic microbalance used was IGAsorp (Intelligent Gravimetric  
126 Analyser Sorption moisture) supplied by Hiden Isochema Limited (UK). At the beginning,  
127 studied RTIL was placed into a glass sample pan, and retained on one end of the electronic  
128 microbalance. The sample environment temperature was controlled by the thermoregulated  
129 water bath and fixed at 25.0 ± 0.2 °C. RTIL was dried by the dry flow of N<sub>2</sub> gas until a  
130 constant mass  $m_0$  was obtained. Then, the water vapor pressure was increased gradually up to  
131 the saturated vapor pressure ( $a = 0.95$ ). At each activity level, the mass gain was continuously  
132 measured as a function of time until an equilibrium state was reached. The water vapor  
133 sorption isotherm was subsequently deduced by plotting the water content at equilibrium  $M$   
134 versus water activity:

135 
$$M = \frac{m_{eq} - m_0}{m_0} = f(a) \quad (\text{Eq. 1})$$

136 where  $m_{eq}$  is the mass at the equilibrium state for a given water activity  $a$ .

137 3) Infrared spectroscopy

138 The infrared measurements were performed using the Fourier transform infrared  
139 (FTIR) Nicolet spectrometer (ThermoFischer, Avatar 360 Omnic Sampler) in an attenuated  
140 total reflectance (ATR) mode (Ge crystal) with a resolution of  $8 \text{ cm}^{-1}$  with 200 scans per  
141 spectrum in the range of  $4000 - 675 \text{ cm}^{-1}$ .

142 The FTIR spectra of RTIL equilibrated with water vapors at a given vapor activity  $a$   
143 were obtained by means of a home-made apparatus developed for that purpose and explained  
144 in details in<sup>26</sup>. In short, dry RTIL was positioned inside a special hood placed over the sample  
145 compartment. The vapor generator was connected to the hood for a few hours, ensuring that  
146 RTIL was in the equilibrium state with the water vapor. Dry nitrogen and water-nitrogen  
147 flows were controlled with an electronic gas flowmeter (Agilent Technologies, 5067 model).  
148 The FTIR spectra were recorded for RTIL equilibrated with the water vapors (from  $a = 0$  (i.e.  
149 dry RTIL) to  $a = 0.95$ ) and liquid water (i.e. at  $a = 1$ ).

150

151 **Theoretical background**

152 1) Two-mode sorption – Henry-clustering

153 The Flory-Huggins thermodynamic theory is used for correlating the penetrant  
154 sorption isotherms<sup>27</sup>. In this case, the sorption isotherm curve exhibits a quasi linear curve at  
155 low ( $a \leq 0.2$ ) and intermediate ( $0.2 < a \leq 0.7$ ) activity and then it is followed by a convex  
156 curvature for higher activity ( $a > 0.7$ ). It is noted that this theory is useful for describing the  
157 water sorption behavior in a hydrophobic material<sup>27</sup>. Usually, the Flory-Huggins theory is  
158 applied for the organic solvent sorption in rubbery materials, for example, the chloroform  
159 sorption in silicone<sup>28</sup>. Perrin *et al.* showed that the water sorption isotherm in hydrophilic  
160 cellulose triacetate could also be well described by the Flory-Huggins theory, but only for the  
161 activity less than  $0.7$ <sup>29</sup>.

162 According to this theory, when a penetrant is added to the material solute, an enthalpy  
163 change can take place as the penetrant-penetrant and solute-solute interactions are replaced by  
164 the penetrant-solute interactions. It should be mentioned that the interactions between the  
165 penetrant and solute are assumed to be constant whatever the penetrant activity. However, the  
166 clustering phenomenon is not clearly explained as the deviation from the Flory-Huggins

167 thermodynamic theory is observed at high penetrant activity ( $\geq 0.7$ ). Therefore, in the case of  
 168 the RTIL water sorption isotherms with a curve shape similar to the Flory-Huggins sorption  
 169 curve shape (i.e. the first linear part followed by the convex shape), it is more judicious to  
 170 describe the isotherm by using an approach, which consists of two sorption modes: the  
 171 Henry's dissolution and the clustering.

172 In the case of a binary system, the penetrant-penetrant and penetrant-material  
 173 interactions are found to be dependent on the penetrant activity value. Thus, in our case it is  
 174 assumed that two species of absorbed water molecules contribute to the water concentration in  
 175 the material (RTIL): one of these species follows the Henry's law at low and intermediate  
 176 water activity ( $0 < a \leq 0.7$ ) (i.e. molecules are randomly sorbed in the medium with no  
 177 specific interaction), and the second of the species at higher activity ( $a > 0.7$ ) follows the  
 178 water clustering (i.e. part of sorbed molecules from the Henry's sorption due to the  
 179 predominant penetrant-penetrant interactions at high water concentration forms a cluster).  
 180 Therefore, taking into account these two combined sorption modes, the water sorption  
 181 isotherm may be expressed as follows:

$$182 \quad C_{H_2O} = C_{(H_2O)_D} + nC_{(H_2O)_n} = k_D a + nK_a k_D^n a^n, \quad (\text{Eq. 2})$$

183 where  $C_{H_2O}$  (g-water/g-RTIL) is the total water concentration,  $C_{(H_2O)_D}$  and  $nC_{(H_2O)_n}$  are the  
 184 water concentration from the Henry's sorption and from the clustered species, respectively,  $a$   
 185 is water activity,  $k_D$  (g-water/g-RTIL) is the Henry's solubility coefficient representing the  
 186 affinity of water molecules to the sample (RTIL),  $n$  is the mean number of water molecules  
 187 per cluster, and  $K_a$  ((g-water/g-RTIL) $^{1-n}$ ) is the equilibrium constant for the clustering  
 188 reaction.

189 The clustering formation corresponds to the next water equilibrium:



191 which is characterized by an equilibrium constant  $K_a$ :

$$192 \quad K_a = \frac{C_{(H_2O)_n}}{C_{H_2O}^n},$$

193 where  $C_{H_2O}$  is the water concentration of free water molecules ( $=k_D a$ ) and  $C_{(H_2O)_n}$  is the  
 194 concentration of the water clusters that can be determined as follows:

$$195 \quad C_{(H_2O)_n} = nK_a C_{H_2O}^n = nK_a k_D^n a^n.$$

196 2) Mean cluster size (MCS)

197 The clustering theory of adsorbed molecules was proposed to explain some of the  
 198 thermodynamic inconsistencies in sorption first by Zimm et Lundberg<sup>30,31</sup> and later by  
 199 Starkweather<sup>32</sup>. Water is unique penetrant due to its polar nature, thus, it can create hydrogen  
 200 bond with itself and can form clusters. This theory allows us to evaluate the degree of  
 201 clustering in binary systems. At this mathematical approach, the clustering function is defined  
 202 as:

$$203 \quad \frac{G_s}{V_s} = -(1 - \Phi_s) \left[ \frac{\partial(a/\Phi_s)}{\partial a} \right]_{p,T} - 1, \quad (\text{Eq. 3})$$

204 where  $G_s$  is the cluster integral,  $V_s$ ,  $\Phi_s$  and  $a$  are the partial molar volume, the volume fraction  
 205 and the activity of penetrant molecules (in our case, water molecules), respectively. The  
 206 clustering function  $\frac{G_s}{V_s}$  indicates whether clustering takes place or not and it can be easily  
 207 determined from the experimental isothermal sorption<sup>33,34</sup>. A  $\frac{G_s}{V_s}$  value equal to -1 (the case  
 208 of the ideal solution, i.e. sorption isotherm following the Henry's law) indicates that penetrant  
 209 molecules do not affect the distribution of other penetrant molecules. If  $\frac{G_s}{V_s} > 0$ , penetrant  
 210 molecules tend to cluster provided the concentration is higher in their neighborhood as it  
 211 would be expected on the basis of non-random mixing, whereas if a  $\frac{G_s}{V_s}$  value is greater than  
 212 -1, penetrant molecules prefer to remain isolated.

213 The expression  $\frac{G_s \Phi_s}{V_s}$  represents the mean number of penetrant molecules in excess  
 214 of the mean concentration. Thus, it measures the clustering tendency of penetrant molecules.  
 215 The MCS value is hence an estimate of the mean number of molecules which exist in a  
 216 cluster:

$$217 \quad MCS = 1 + \left[ \frac{\Phi_s G_s}{V_s} \right] \quad (\text{Eq. 4})$$

218 Following Starkweather<sup>32</sup>, the equation for the mean size of a cluster can be written as:

$$219 \quad MCS = (1 - \Phi_s) \frac{a}{\Phi_s} \left( \frac{\partial \Phi_s}{\partial a} \right)_{p,T} \quad (\text{Eq. 5})$$



220 The volume fraction  $\Phi_s$  is obtained from the relation:

$$221 \quad \Phi_s = \left( 1 + \frac{\rho_s}{M\rho_{IL}} \right)^{-1}, \quad (\text{Eq. 6})$$

222 where  $\rho_s$  and  $\rho_{IL}$  are the densities of the penetrant (water) and sample (RTIL), respectively.  
223 The mass uptake  $M$  at the equilibrium and at a given activity  $a$  of sorbed species is defined  
224 according to Eq. 1. In the case of the Henry-clustering mode, the mass uptake can be  
225 expressed according to Eq. 2.

226 In the case of water transport studies, the Zimm and Lundberg theory has been often  
227 coupled with the approaches that allow obtaining a mathematical description of the water  
228 sorption isotherms. As a result, the MCS value can be expressed from the Henry-clustering  
229 parameters as follows:

$$230 \quad MCS = \frac{\rho^2}{M^3 \left( 1 + \frac{\rho}{M} \right)^2} (k_D a + n^2 K_a k_D^n a^n), \quad (\text{Eq. 7})$$

231 where  $\rho = \frac{\rho_s}{\rho_{IL}}$ . The densities of studied RTILs are 1.25 g/cm<sup>3</sup> for [C<sub>6</sub>Py][PF<sub>6</sub>], 1.31 g/cm<sup>3</sup>  
232 for [C<sub>6</sub>C<sub>1</sub>im][PF<sub>6</sub>] and 1.21 g/cm<sup>3</sup> for [C<sub>4</sub>C<sub>1</sub>im][BF<sub>4</sub>].

233

## 234 **Results and discussion**

### 235 1) Water sorption

236 The sorption kinetics of water vapor into a material depends on numerous factors, such  
237 as the chemical composition, the physical and chemical properties, etc. A continuous  
238 gravimetric analysis was performed in order to understand possible interactions of water  
239 molecules and [C<sub>6</sub>Py][PF<sub>6</sub>] over the whole range of water activity. Fig. 2 shows that the  
240 experimental data of the water vapor sorption kinetics of [C<sub>6</sub>Py][PF<sub>6</sub>] depend directly on the  
241 water activity  $a$ . As one can see, the water uptake increases with time to the achievement of  
242 the sorption equilibrium after certain period of time. Besides, the maximal amount of sorbed  
243 water increases when the water activity  $a$  increases. Moreover, the sorption kinetics becomes  
244 longer starting from  $a = 0.8$ . Before this value, the equilibrium state (i.e. gain mass plateau  
245 value) is reached rather rapidly (Fig. 2). The sorption kinetics provides a valuable insight into  
246 the mechanism involved in the transport of penetrate within a material. In order to get the  
247 details of the water sorption kinetics into RTIL, the water vapor sorption isotherm was  
248 obtained from the mass gain at the equilibrium state of the sorption kinetics according to Eq. 1

249 (Fig. 3). The water vapor sorption isotherms of imidazolium-based RTILs ([C<sub>6</sub>C<sub>1</sub>im][PF<sub>6</sub>] and  
250 [C<sub>4</sub>C<sub>1</sub>im][BF<sub>4</sub>]) (Fig. 1) obtained on the same conditions are added for comparison. The  
251 choice of [C<sub>6</sub>C<sub>1</sub>im][PF<sub>6</sub>] is based on the fact that this RTIL is a well-known example of water-  
252 immiscible RTILs<sup>1,2,14,15,19,35</sup> and is known to have very weak interactions with water  
253 molecules even at high water activity, whereas [C<sub>4</sub>C<sub>1</sub>im][BF<sub>4</sub>] is water-miscible  
254 RTIL<sup>1,2,14,15,19,35</sup> and is known for its strong water interaction capacity leading to the water  
255 clustering at high activity.

256 It can be seen from Fig. 3 that the water uptake by [C<sub>6</sub>Py][PF<sub>6</sub>] is quasi-linear and  
257 non-specific at low and intermediate water activity (up to  $a < 0.8$ ), whereas at high water  
258 activity ( $a > 0.8$ ), the water uptake increases exponentially.

259 The analysis of an adequate sorption isotherm model can give important information  
260 concerning the water organisation in the material. The water vapour isotherms have been  
261 already exploited and treated by classical thermodynamic models such as local-composition  
262 models, Group Contribution Methods<sup>36</sup>, COSMO<sup>37</sup> and by other less classical models such as  
263 the modified RK EOS<sup>38</sup> and the Camper model<sup>39</sup>. As to the so-called local-composition  
264 models, one can find the non-random two-liquid model (NRTL)<sup>40-42</sup>, the Wilson model<sup>43</sup>, the  
265 UNIQUAC model<sup>44,45</sup>, and the group contribution model UNIFAC<sup>46</sup>, but also GAB<sup>47-49</sup> and  
266 Park<sup>50,51</sup> models. Among all proposed in the literature models, it is admitted that GAB model  
267 is mostly used to describe the water sorption by food and food-stuffs. In the case of an  
268 exponential increase of the solvent concentration at high vapor pressure (i.e. in the case of the  
269 convex form of the isotherm) some other models can be also applied, e.g. Flory-Huggins,  
270 ENSIC, or aggregation models. For example, the Flory-Huggins model (usually used for  
271 vapor sorption in rubbery-elastomer materials) is not appropriate for polar penetrants such as  
272 water molecules (according to hypothesis of Flory-Huggins), so this model cannot be used for  
273 the ionic liquid/water system studied in the present work. The convex form of the isotherm is  
274 usually attributed to the typical water clustering phenomenon, and the strong increase of the  
275 water concentration at high water vapor pressure values is explained by the water/water  
276 interactions, which become predominant, compared to the water/substrate interactions. It is  
277 well known that such phenomenon occurs mainly in polar systems (i.e. in the case of  
278 hydrophilic materials) or in the system containing ionic groups, which are able to interact with  
279 water molecules, e.g. polyelectrolyte (Nafion<sup>®</sup>). In addition, as ionic liquids are liquid salts,  
280 so ion pairs can be easily solvated by water molecules, thus forming a hydration shell.  
281 Recently Zhu et al showed by means of a detailed NMR analysis that imidazolium cations  
282 with no or short alkyl chains can form a self-assembled clustering structure in water

283 solution<sup>52</sup>. The authors revealed the presence of the first hydration shell of the polar heads of  
284 cations at the water concentration around 60 mol.%. Owing to the high mobility of ionic  
285 liquids (i.e. low viscosity compared to polymer material), it is reasonable to imagine that  
286 water molecules move and are bonded with each other by strong hydrogen bonds as in bulk  
287 liquid water.

288 The presence of water clusters in ionic liquids is the well-known fact and it is  
289 confirmed by both theoretical and experimental points of view. Being based on computation  
290 studies of three ionic liquid systems containing [BF<sub>4</sub>], [PF<sub>6</sub>] and [Tf<sub>2</sub>N] anions, Maiti et al.  
291 revealed that the inclusion of small hydrogen-bonded water clusters was in better quantitative  
292 agreement with the experimentally observed water sorption data<sup>53</sup>. Also, molecular dynamics  
293 simulation (MDS) of mixtures of 1,3-dialkyl imidazolium ionic liquids and water performed  
294 by Hanke and Lynden-Bell has shown that when the molar proportion of water molecules  
295 reached 75%, a percolating network of water and small clusters was formed<sup>54</sup>. Singh and  
296 Kumar examined the cation-anion-water interactions in aqueous mixtures of imidazolium  
297 ionic liquids over the whole composition range using FTIR spectroscopy<sup>55</sup>. They showed the  
298 existence of the hydration shell for [BF<sub>4</sub>] anion and deduced the presence of water clusters  
299 from the overall broad structure of the -OH band at 2800-3800 cm<sup>-1</sup>. Moreover, by comparing  
300 MDS results with the NMR data, Moreno et al. clearly showed that the ions were selectively  
301 coordinated by individual water molecules at low water content, while the ionic network was  
302 disrupted by the water clusters at high water content<sup>56</sup>.

303 Taking into account the literature results mentioned above, in the present article the  
304 dual-mode (Henry and clustering) was chosen. To evaluate how accurate the fitting was,  
305 residual sum of squares (RSS) was used, i.e. the sum of squares of residuals (i.e. deviations  
306 predicted from actual empirical values of data). RSS value allows measuring the discrepancy  
307 between the experimental data and the estimation model. In each case, very small RSS values  
308 were obtained indicating an accurate fit of the model to the experimental data. The fitted  
309 model parameters ( $k_D$ ,  $K_a$  and  $n$ ) (Eq. 2) are gathered in Table 1.

310 At low and intermediate water activity ( $a \leq 0.8$ ), the water uptake by [C<sub>6</sub>Py][PF<sub>6</sub>]  
311 increases linearly with the water activity value, revealing the typical Henry's sorption mode  
312 (the first term in Eq. 2), for which interactions between water molecules are not predominant.  
313 This sorption mode assumes a random dispersion of sorbed water molecules in RTIL. The  
314 Henry's coefficient  $k_D$  calculated from the curve slope illustrates the affinity of water  
315 molecules and RTIL. The higher is the  $k_D$  value, the higher is the water solubility in RTIL.  
316 From the thermodynamical point of view, the [C<sub>6</sub>Py][PF<sub>6</sub>] water uptake is very low and quite

317 similar to that of [C<sub>6</sub>C<sub>1</sub>im][PF<sub>6</sub>] (Fig. 3), thus confirming their hydrophobic character. It can  
318 be noted that the  $k_D$  values of [C<sub>6</sub>Py][PF<sub>6</sub>] and [C<sub>6</sub>C<sub>1</sub>im][PF<sub>6</sub>] are rather close (Table 1) that  
319 explains the superposition of the water vapor sorption isotherms up to  $a = 0.8$  (Fig. 3). It can  
320 be seen from Fig. 3 that the amount of water absorbed by [C<sub>4</sub>C<sub>1</sub>im][BF<sub>4</sub>] is largely higher than  
321 that absorbed by two [PF<sub>6</sub>]-based RTILs at low and intermediate water activity. As a result,  
322 the  $k_D$  value of [C<sub>4</sub>C<sub>1</sub>im][BF<sub>4</sub>] is almost ten times higher compared to that of [C<sub>6</sub>Py][PF<sub>6</sub>]  
323 (Table 1). Thus, one can conclude that water molecules have very few interactions with  
324 [C<sub>6</sub>Py][PF<sub>6</sub>] at low and intermediate activity, and that the behavior of [C<sub>6</sub>Py][PF<sub>6</sub>] towards  
325 water is very similar to that of [C<sub>6</sub>C<sub>1</sub>im][PF<sub>6</sub>] (water-immiscible RTIL). This fact is in good  
326 agreement with the research of Papaiconomou *et al.*<sup>24</sup>, who studied the water solubility of  
327 RTILs containing octylpyridinium-type cations, and found them nearly water immiscible. In  
328 addition, numerous studies indicate a weak water miscibility of [PF<sub>6</sub>]-based RTILs because of  
329 the [PF<sub>6</sub>] anion presence<sup>1,2,14,15,19,35</sup>. Furthermore, it is interesting to note that [C<sub>6</sub>Py][PF<sub>6</sub>] and  
330 [C<sub>6</sub>C<sub>1</sub>im][PF<sub>6</sub>] present almost the same interactions with water molecules up to  $a = 0.8$  (Fig.  
331 3), although the chemical structure of their cations is different (Fig. 1). It means that at low  
332 and intermediate water activity (i.e. at  $a < 0.8$ ) the dialkylimidazolium cations and  
333 alkylpyridinium cations have approximately the same influence on the water sorption  
334 properties of RTILs (for the same anion). This result is consistent with the study of Neves *et*  
335 *al.*<sup>21</sup>, who noted that the water solubility in 1-methyl-3-propylimidazolium and 1-methyl-3-  
336 propylpyridinium cations combined with the [PF<sub>6</sub>] anion is similar at 30°C.

337 At high water activity ( $a > 0.8$ ), the strong increase in the [C<sub>6</sub>Py][PF<sub>6</sub>] water uptake  
338 reveals the water clustering formation, which occurs also in [C<sub>4</sub>C<sub>1</sub>im][BF<sub>4</sub>] (Fig. 3).  
339 Consequently, the values of  $K_a$  (the equilibrium constant for the clustering reaction) and  $n$  (the  
340 mean number of water molecules per cluster) for these two RTILs are significantly higher in  
341 comparison with those for [C<sub>6</sub>C<sub>1</sub>im][PF<sub>6</sub>] (Table 1). Moreover, the values of  $K_a$  and  $n$  for  
342 [C<sub>6</sub>Py][PF<sub>6</sub>] are surprisingly higher than those for [C<sub>4</sub>C<sub>1</sub>im][BF<sub>4</sub>], which is water-miscible  
343 RTIL. This means that water molecules are aggregated more easily in [C<sub>6</sub>Py][PF<sub>6</sub>] than in  
344 [C<sub>4</sub>C<sub>1</sub>im][BF<sub>4</sub>]. This result is very interesting, indicating, on the one hand, that the  
345 hydrophobicity of the cation increases from imidazolium- to pyridinium-based RTILs<sup>21,22</sup> and,  
346 on the other hand, that the role of anion in the water sorption and clustering in RTILs is a key  
347 one<sup>14-16,18,19,35,44,55</sup>. Indeed, it is well known that the [BF<sub>4</sub>] anion, compared to the [PF<sub>6</sub>] one,  
348 promotes the strong hydrogen bonds with and between water molecules<sup>14,15,19,55,57</sup>, which  
349 explains both the strong water uptake and the formation of the water clusters in [BF<sub>4</sub>]-based  
350 RTILs, compared to [PF<sub>6</sub>]-based RTILs. These literature findings seem not to be valid for all

351 types of RTILs, but they are more suitable only for some classes of RTILs, such as  
352 imidazolium-based RTILs (the most extensively studied class in the literature). Consequently,  
353 it is not sufficient to take only the anion nature as an indicator of water miscibility in RTILs  
354 as it is shown in the present study that [C<sub>6</sub>Py][PF<sub>6</sub>] which is [PF<sub>6</sub>]-based RTIL has the highest  
355 values of  $K_a$  and  $n$  (Table 1) revealing an easier capacity for water molecules clustering  
356 compared to [C<sub>4</sub>C<sub>1</sub>im][BF<sub>4</sub>] (which is [BF<sub>4</sub>]-based RTIL). This result could be due to the  
357 stronger dispersive interactions and, simultaneously, to the decreasing of cohesivity in  
358 pyridinium-based RTILs than in imidazolium-based RTILs<sup>25</sup>. The different kinds of water  
359 interactions with the  $\pi$  systems of aromatic cations (pyridinium and imidazolium cations) will  
360 be also responsible for this result<sup>58</sup>.

361 The [C<sub>6</sub>Py] cation is of importance in the water clustering formation, even in  
362 combination with the [PF<sub>6</sub>] anion. This fact highlights the strong influence of the cation  
363 nature, in addition to that of anion, on the water sorption and clustering in pyridinium-based  
364 RTILs. Therefore, it is essential that the cation nature must be also taken into account in the  
365 study of interactions of water molecules and pyridinium-based RTILs. On the other hand, it is  
366 shown that [C<sub>6</sub>Py][PF<sub>6</sub>] has a very low affinity towards water molecules at low and  
367 intermediate activity (the  $k_D$  value (Table 1)). Thus, the behavior of pyridinium-based RTIL  
368 towards water molecules can be changed depending on water activity: [C<sub>6</sub>Py][PF<sub>6</sub>] is water-  
369 immiscible RTIL at low and intermediate activity, thus limiting the water sorption, but at high  
370 activity ( $a > 0.8$ ) the further sorption of water molecules on already sorbed monolayer  
371 moisture favours the water clustering formation as with the water activity increasing  
372 water/water interactions are largely stronger than water/RTIL ones. So, starting from a certain  
373 water concentration water molecules are self-associated to form clusters. Such behavior has  
374 been also observed in the case of the water sorption in low density polyethylene<sup>59</sup>. Indeed, the  
375 water cluster formation is revealed in this hydrophobic polymer with very low affinity  
376 towards polar molecules. The water clustering is explained by the hydrogen bonds between  
377 water molecules themselves confined in the matrix, thus leading to further reducing of the  
378 water mobility through the material. Therefore, for each given RTIL application, it is  
379 important first to determine the necessary water activity range. If the water presence in  
380 [C<sub>6</sub>Py][PF<sub>6</sub>] is not desired at all, the operating conditions should be in the water activity range  
381 less than 0.8 in order to avoid the water sorption and clustering formation as much as  
382 possible. On the contrary, if the water presence is required, the RTIL can be applied at the  
383 water activity value close to 1. For other applications using pyridinium-based RTILs and  
384 where water is the reaction media (or is used in large quantity), the replacement of the [PF<sub>6</sub>]

385 anion by others anions is recommended to further improve the water miscibility of RTIL.  
386 Popov *et al.*<sup>60</sup> used *N*-butyl-4-methyl-pyridinium tetrafluoroborate in aqueous solutions to  
387 measure the stability constants of crown-ether complexes with alkali-metal ions. This RTIL  
388 was qualified by Wang *et al.*<sup>61</sup> as water-soluble RTIL. It was used as a co-solvent with water  
389 by Riva *et al.*<sup>62</sup> to separate aromatic hydrocarbons from a naphtha of very low-aromatic-  
390 content (10 wt.%). Indeed, it is known that the different behavior of the [BF<sub>4</sub>] and [PF<sub>6</sub>]  
391 anions is attributed to the fact that the [BF<sub>4</sub>] van der Waals volume (48 Å<sup>3</sup>) is smaller than the  
392 [PF<sub>6</sub>] one (68 Å<sup>3</sup>), that gives more space for water molecules to be accommodated in [BF<sub>4</sub>]-  
393 based RTILs<sup>16,63</sup>. Papaiconomou *et al.*<sup>24</sup> measured the water content of air-saturated and  
394 water-saturated pyridinium RTILs, 1-octyl-4-methylpyridinium tetrafluoroborate  
395 ([4C<sub>1</sub>C<sub>8</sub>Py][BF<sub>4</sub>]), 1-octyl-2-methylpyridinium tetrafluoroborate ([2C<sub>1</sub>C<sub>8</sub>Py][BF<sub>4</sub>]), 1-octyl-4-  
396 methylpyridinium trifluoromethyl sulfonate ([4C<sub>1</sub>C<sub>8</sub>Py][TfO]), and 1-octyl-4-  
397 methylpyridinium dicyanamide ([4C<sub>1</sub>C<sub>8</sub>Py][N(CN)<sub>2</sub>]). At the equilibrium state with liquid  
398 water, the water content (in mass fraction) is 11.3, 13.6, 17.2 and 54.9% for [4C<sub>1</sub>C<sub>8</sub>Py][BF<sub>4</sub>],  
399 [2C<sub>1</sub>C<sub>8</sub>Py][BF<sub>4</sub>], [4C<sub>1</sub>C<sub>8</sub>Py][TfO] and [4C<sub>1</sub>C<sub>8</sub>Py][N(CN)<sub>2</sub>], respectively. These values are  
400 much higher compared to 10.2% obtained for [C<sub>6</sub>Py][PF<sub>6</sub>] at  $a = 0.95$ . These pyridinium-  
401 based RTILs are, therefore, more water-miscible than [C<sub>6</sub>Py][PF<sub>6</sub>] obviously due to the  
402 combination of the pyridinium-based cation with such anions as [BF<sub>4</sub>], [TfO] and [N(CN)<sub>2</sub>].

403 Another question which arises is whether the water clustering mechanism in  
404 [C<sub>6</sub>Py][PF<sub>6</sub>] is the same as in [C<sub>4</sub>C<sub>1</sub>im][BF<sub>4</sub>] (as no clustering is observed in [C<sub>6</sub>C<sub>1</sub>im][PF<sub>6</sub>]  
405 (see Fig. 3)). Fortunato *et al.*<sup>63,64</sup> studied the water uptake of imidazolium-based RTILs after  
406 their contact with aqueous solutions. The authors concluded that water molecules began to  
407 cluster on the molecular level only when the water content in RTIL exceeded a certain critical  
408 concentration. Scovazzo<sup>65</sup> indicated that the critical concentration for the water cluster  
409 formation is easier to reach for the water-miscible RTILs than for the water-immiscible  
410 RTILs. Dahi *et al.*<sup>57</sup> showed that the clustering process was linked to the affinity of water  
411 molecules and RTIL already at low and intermediate water activity: the higher the  $k_D$  value,  
412 the higher the probability of the water clustering at high activity. From the obtained  $k_D$  values  
413 (Table 1), it is clearly seen that the affinity or interactions of water molecules are very low in  
414 the case of [C<sub>6</sub>C<sub>1</sub>im][PF<sub>6</sub>] and rather high for [C<sub>4</sub>C<sub>1</sub>im][BF<sub>4</sub>] at low and intermediate water  
415 activity. This result allows us to explain why water molecules easily formed the clusters in  
416 [C<sub>4</sub>C<sub>1</sub>im][BF<sub>4</sub>] (high  $K_a$  value, Table 1) in contrast with [C<sub>6</sub>C<sub>1</sub>im][PF<sub>6</sub>] (low  $K_a$  value, Table  
417 1) at high water activity. Indeed, it is known that the [BF<sub>4</sub>] anion promotes the strong  
418 hydrogen bonds with and between water molecules imidazolium-based RTILs compared to

419 the [PF<sub>6</sub>] anion<sup>14,15,19,44,55,57</sup>, which explains both the strong water uptake and the formation of  
420 the water clusters in [C<sub>4</sub>C<sub>1</sub>im][BF<sub>4</sub>] compared to [C<sub>6</sub>C<sub>1</sub>im][PF<sub>6</sub>]. However, in the case of  
421 [C<sub>6</sub>Py][PF<sub>6</sub>] (pyridinium-based RTIL), despite the low affinity with water at low and  
422 intermediate water activity (low  $k_D$  value (Table 1), water molecules can easily form clusters  
423 in this RTIL at high activity, even more easily compared to [C<sub>4</sub>C<sub>1</sub>im][BF<sub>4</sub>] (compare the  $K_a$   
424 values (Table 1)). Combining these results with the studies of Fortunato *et al.*<sup>63,64</sup>, Scovazzo<sup>65</sup>  
425 and Dahi *et al.*<sup>57</sup>, it can be pointed out that the water clustering mechanism in [C<sub>6</sub>Py][PF<sub>6</sub>] is  
426 different from that in [C<sub>4</sub>C<sub>1</sub>im][BF<sub>4</sub>]. It seems that in the case of [C<sub>6</sub>Py][PF<sub>6</sub>], which is  
427 alkylpyridinium-based RTIL, the critical concentration for the water clustering formation is  
428 much lower in comparison to imidazolium-based RTILs. This fact may be explained by the  
429 RTIL cation structure. Wang *et al.*<sup>58</sup> studied hydrogen bonding interactions of 1-  
430 butylpyridinium tetrafluoroborate [C<sub>4</sub>Py][BF<sub>4</sub>] and water. They stated that water, when it  
431 forms the strong anion-HOH-anion complex, could also form H-bonds with aromatic C-H  
432 bond on the [C<sub>4</sub>Py] cation. This result is different from the case of imidazolium-based RTILs,  
433 where the strong anion-cation interaction and steric hindrance from the alkyl chain length  
434 prevent water molecules to form H-bonding with aromatic C-H on the imidazolium cation,  
435 thus favouring interactions with the anion. This observation supports well the previously  
436 mentioned hypothesis about much stronger interactions of water molecules and the  $\pi$  systems  
437 of the pyridinium cations than of water molecules and the imidazolium cations.

438 In order to determine the activity from which the water clusters started to form in  
439 RTILs, the MCS value (Eq. 7) was calculated in addition to the  $n$  parameter (Eq. 2), which  
440 represents roughly the number of water molecules per cluster. The calculated MCS values  
441 were plotted as a function of the water activity  $a$  (Fig. 4). The MCS values are found to be  
442 close to unity at low water activity (below  $a = 0.6$ ) for all three studied RTILs and clustering  
443 does not take place in this region. Then, the MCS values start to increase rapidly for  
444 [C<sub>6</sub>Py][PF<sub>6</sub>] and [C<sub>4</sub>C<sub>1</sub>im][BF<sub>4</sub>], whereas for [C<sub>6</sub>C<sub>1</sub>im][PF<sub>6</sub>] they stay still very low ( $\sim 2$  at  $a =$   
445  $0.95$ ). Such a result is expected as [C<sub>6</sub>C<sub>1</sub>im][PF<sub>6</sub>] is water-immiscible RTIL over the whole  
446 range of water activity.

447 According to the Zimm-Lundberg theory, the MCS value greater than one is an  
448 indication of the cluster formation<sup>30,31</sup>. Thus, one can conclude that the water clustering starts  
449 from  $a = 0.7-0.8$  for [C<sub>6</sub>Py][PF<sub>6</sub>] and [C<sub>4</sub>C<sub>1</sub>im][BF<sub>4</sub>]. Starting from  $a \approx 0.8$ , further sorption of  
450 water molecules leads to the enhancement of water/water interactions and, thus, to the cluster  
451 formation. The formed hydrogen bonds between water molecules promote the rapid formation  
452 of a compact hydrogen bond network<sup>57</sup>, which triggers the water clustering. As it can be seen

453 from Fig. 3, at  $a = 0.8$  the water sorption obtained for [C<sub>4</sub>C<sub>1</sub>im][BF<sub>4</sub>] (0.1075 g water/g RTIL)  
454 is higher than that for [C<sub>6</sub>Py][PF<sub>6</sub>] (0.017 g water/g RTIL). At the same time, with the  
455 increase of water activity above 0.8, the MSC value increases much faster in the case of  
456 [C<sub>6</sub>Py][PF<sub>6</sub>] compared to [C<sub>4</sub>C<sub>1</sub>im][BF<sub>4</sub>] (Fig. 4). It means that the water clustering process is  
457 more pronounced in [C<sub>6</sub>Py][PF<sub>6</sub>] than in [C<sub>4</sub>C<sub>1</sub>im][BF<sub>4</sub>], thus allowing us to obtain rapidly  
458 larger water clusters in [C<sub>6</sub>Py][PF<sub>6</sub>]. This indicates again that the water clustering mechanism  
459 in [C<sub>6</sub>Py][PF<sub>6</sub>] is different from that in [C<sub>4</sub>C<sub>1</sub>im][BF<sub>4</sub>]. The obtained MCS plots based on the  
460 Zimm-Lundberg theory agree very well with the results of the Henry-clustering model.  
461 Indeed, the MCS value is equivalent to the  $n$  parameter (the mean number of water molecules  
462 per cluster). However, the  $n$  value depends strongly on the quality of the fit of the  
463 experimental data and, so, gives only an approximation of the cluster size (i.e. the average  
464 value), whereas the MCS value, derived from the statistical mechanics analysis, allows us to  
465 determine more precisely the mean size of cluster which varies with the environmental  
466 activity. From Fig. 4, one can easily see that the maximum value of MCS (at  $a = 0.95$ )  
467 determined for [C<sub>6</sub>Py][PF<sub>6</sub>], [C<sub>4</sub>C<sub>1</sub>im][BF<sub>4</sub>] and [C<sub>6</sub>C<sub>1</sub>im][PF<sub>6</sub>] is  $\sim 22$ , 12 and 2, respectively.  
468 These values are in good agreement with the calculated  $n$  values (25, 19 and 3, respectively,  
469 Table 1), thus confirming the same tendency. The highest values of MCS and  $n$  are found for  
470 [C<sub>6</sub>Py][PF<sub>6</sub>] indicating a strong trend of water molecules to form clusters of large size (more  
471 than 20 water molecules per cluster) in this RTIL at high water activity.

472

## 473 2) Water molecular state

474 The measurement of the water clustering and interactions in a material is a key factor,  
475 however, the proposed structures and/or functions of water differ in many cases, and little  
476 consistency can be found among structures. Therefore, the water uptake should be also  
477 characterized by direct measurements using the infrared spectroscopy, where -OH bonds for  
478 different water populations have distinct bands and can be individually distinguished.

479 The IR bands corresponded to the water stretching vibration modes are widely used to  
480 study the molecular state of water dissolved in various solvents<sup>66,67</sup>. Two characteristic IR  
481 bands exist in the region of 3000-3800 cm<sup>-1</sup>: the antisymmetric ( $\nu_3$ ) and symmetric ( $\nu_1$ )  
482 stretching modes. Their intensity and position are strongly influenced both by the water  
483 environment and the water association *via* hydrogen bonding<sup>14,19,55,57</sup>. For example, in the  
484 case of the water vapor when water molecules are distant from each other, the  $\nu_3$  and  $\nu_1$  bands  
485 are situated at 3756 and 3657 cm<sup>-1</sup>, respectively. In this case, water molecules are free (i.e.



486 they are not associated by hydrogen bonds). On the contrary, in the case of the liquid water,  
487 water molecules are linked by hydrogen bonds and these interactions trigger the overlapping  
488 of the  $\nu_3$  and  $\nu_1$  bands leading to a broad and intense band with a maximum at around 3300  
489  $\text{cm}^{-1}$ .

490 Fig. 5 shows the ATR-FTIR spectra of  $[\text{C}_6\text{Py}][\text{PF}_6]$  in the region of the  $\nu(\text{OH})$   
491 stretching modes of water ( $3000\text{-}3800\text{ cm}^{-1}$ ) obtained at different water activity. At the  
492 beginning,  $[\text{C}_6\text{Py}][\text{PF}_6]$  was dried by the nitrogen flow ( $a = 0$ ) in order to remove any residual  
493 water molecules. As a result, no characteristic IR bands of water were observed in the region  
494  $3000\text{-}3800\text{ cm}^{-1}$  (Fig. 5). Then,  $[\text{C}_6\text{Py}][\text{PF}_6]$  was progressively equilibrated at various water  
495 activity values (from 0 to 1).

496 No significant changes were noticed on the IR spectra up to  $a = 0.82$ . The absence of  
497 the water characteristic bands on the IR spectra of RTIL in the activity range from 0 to 0.8  
498 may be explained by the very low water content in  $[\text{C}_6\text{Py}][\text{PF}_6]$ . This result confirms that  
499  $[\text{C}_6\text{Py}][\text{PF}_6]$  is water-immiscible RTIL at  $0 < a < 0.8$ . On the contrary, when  $[\text{C}_6\text{Py}][\text{PF}_6]$  is  
500 equilibrated with water vapors at  $a = 0.88$ , a broad and intense band appears at  $3360\text{ cm}^{-1}$   
501 (Fig. 5). The high intensity of this band and rapidity of its appearance proves a rapid and  
502 strong increase of the water content in  $[\text{C}_6\text{Py}][\text{PF}_6]$  from  $a = 0.82$  to  $a = 0.88$ . The sorption of  
503 a higher quantity of water molecules enhances significantly water/water interactions. As a  
504 result, sorbed water molecules start to interact together by hydrogen bonds. The shape and  
505 position of the band confirm the presence of intermolecular forces between water molecules,  
506 as the intense band results from the overlapping of the  $\nu_3$  and  $\nu_1$  bands<sup>14,19,55,57</sup>. Therefore,  
507 water molecules are well associated by hydrogen bonds at  $a = 0.88$ . This clustering starts  
508 probably even at  $a = 0.82$  as the appearance of a large band around  $3300\text{ cm}^{-1}$  can be already  
509 observed on the spectrum at this water activity value (Fig. 5). This fact means that the activity  
510 value around 0.8 marks a crucial point in the behavior of  $[\text{C}_6\text{Py}][\text{PF}_6]$  towards water. This  
511 observation conforms well to the MCS results (compare Fig. 4 and 5). The formed hydrogen  
512 bonds between water molecules promote the formation of a compact hydrogen bond  
513 network<sup>57</sup> and, subsequently, the formation of the water clusters. On the other hand, it does  
514 not seem necessary to reach a critical water content in  $[\text{C}_6\text{Py}][\text{PF}_6]$  for the water association  
515 by hydrogen bonds and the formation of the water clustering since  $[\text{C}_6\text{Py}][\text{PF}_6]$  reveals a low  
516 water content already at  $a = 0.82$  (Fig. 5). This fact confirms the hypothesis proposed above  
517 that the water clustering mechanism in  $[\text{C}_6\text{Py}][\text{PF}_6]$  is different from that in imidazolium-  
518 based RTILs. The increasing of water activity up to 1 promotes the increase of the intensity

519 and width of the water band (Fig. 5), i.e. further strengthening the hydrogen bond network.  
520 Consequently, water molecules sorbed in [C<sub>6</sub>Py][PF<sub>6</sub>] form clusters or even droplets of the  
521 bulk liquid-like water at high water activity value. In addition, the shape of the band remains  
522 unchanged with the water activity increase, which would indicate that the molecular state of  
523 water in [C<sub>6</sub>Py][PF<sub>6</sub>] is independent of the water concentration. According to numerous  
524 studies<sup>14,17,55,57,68,69</sup>, the intense and broad band in the region around 3400 cm<sup>-1</sup> is attributed to  
525 water clusters. At high activity ( $a > 0.8$ ), water in [C<sub>6</sub>Py][PF<sub>6</sub>] shows undoubtedly an easier  
526 capacity to be associated by hydrogen bonds until the water clustering formation.

527 The molecular state of water dissolved in different RTILs was studied by means of the  
528 infrared spectroscopy as a function of water activity<sup>57</sup>. Water molecules dissolved in  
529 [C<sub>4</sub>C<sub>1</sub>im][PF<sub>6</sub>] and [C<sub>6</sub>C<sub>1</sub>im][PF<sub>6</sub>] (water-immiscible RTILs) were found to be not self-  
530 associated by hydrogen bonds whatever the water content and, thus, they can be assigned as  
531 free water molecules. On the contrary, water molecules sorbed in [C<sub>4</sub>C<sub>1</sub>im][BF<sub>4</sub>],  
532 [C<sub>4</sub>im][dibutylphosphate], [C<sub>4</sub>im][bis(2-ethylhexyl)phosphate] and [Et<sub>3</sub>HN][CF<sub>3</sub>SO<sub>3</sub>] (water-  
533 miscible RTILs) were strongly associated with each other by the hydrogen bonds, and could  
534 be easily aggregated at high water activity. In the present study, although [C<sub>6</sub>Py][PF<sub>6</sub>] is  
535 [PF<sub>6</sub>]-based RTIL like [C<sub>4</sub>C<sub>1</sub>im][PF<sub>6</sub>] and [C<sub>6</sub>C<sub>1</sub>im][PF<sub>6</sub>], its behavior towards water at high  
536 activity is similar to that of above-mentioned water-miscible RTILs. The obtained IR results  
537 are in good agreement with the gravimetric analysis and the MCS results, and confirm the  
538 dual behavior of [C<sub>6</sub>Py][PF<sub>6</sub>]: water-immiscible RTIL from  $a = 0$  to  $a = 0.8$ , and water-  
539 miscible RTIL at  $a > 0.8$ .

540

## 541 **Conclusion**

542 The water sorption properties of 1-hexylpyridinium hexafluorophosphate [C<sub>6</sub>Py][PF<sub>6</sub>]  
543 were successfully investigated over the whole range of water activity. The experimental data  
544 of the water sorption isotherm were well fitted with the two-mode Henry-clustering model,  
545 and compared to those of imidazolium-based RTILs – [C<sub>4</sub>C<sub>1</sub>im][BF<sub>4</sub>] and [C<sub>6</sub>C<sub>1</sub>im][PF<sub>6</sub>]. At  
546 low and intermediate water activity ( $0 < a < 0.8$ ), the mass uptake was weak and,  
547 consequently, the affinity of water molecules and [C<sub>6</sub>Py][PF<sub>6</sub>] was rather low. On the  
548 contrary, at  $a > 0.8$  the water uptake increases exponentially until the water clustering  
549 formation. The obtained results revealed that the water clustering mechanism in [C<sub>6</sub>Py][PF<sub>6</sub>]  
550 is different from that in imidazolium-based RTILs. This proves the important influence of the  
551 cation structure, in addition to that of anion, on the water sorption of pyridinium-based RTILs.

552 The MCS values calculated according to the Zimm-Lundberg theory for [C<sub>6</sub>Py][PF<sub>6</sub>],  
553 [C<sub>6</sub>C<sub>1</sub>im][PF<sub>6</sub>] and [C<sub>4</sub>C<sub>1</sub>im][BF<sub>4</sub>] were in good agreement with the results obtained by the  
554 Henry-clustering model. Both results indicate a strong trend of the water clustering in  
555 [C<sub>6</sub>Py][PF<sub>6</sub>] starting from  $a = 0.8$ . This trend is much more pronounced than in [C<sub>4</sub>C<sub>1</sub>im][BF<sub>4</sub>]  
556 (water-miscible RTIL). It is concluded that the water sorption capacity of [C<sub>6</sub>Py][PF<sub>6</sub>] varies  
557 so much with water activity that it can be considered as water-immiscible RTIL at the low and  
558 intermediate activity ( $0 < a \leq 0.8$ ), and water-miscible RTIL at high water activity ( $a > 0.8$ ).

559 The results of the sorption measurements were correlated with the molecular state of  
560 water dissolved in [C<sub>6</sub>Py][PF<sub>6</sub>] studied by the infrared spectroscopy. At low and intermediate  
561 activity ( $a \leq 0.8$ ), the water concentration in [C<sub>6</sub>Py][PF<sub>6</sub>] was found to be low and, hence,  
562 [C<sub>6</sub>Py][PF<sub>6</sub>] showed the behaviour of water-immiscible RTIL. On the contrary, at high  
563 activity ( $a > 0.8$ ), the water concentration in [C<sub>6</sub>Py][PF<sub>6</sub>] significantly increased. Water  
564 molecules were strongly associated with each other by the hydrogen bonds leading to the  
565 formation of a compact hydrogen bond network. Accordingly, water can easily form clusters.  
566 At high activity, [C<sub>6</sub>Py][PF<sub>6</sub>] showed the behaviour of water-miscible RTIL. Although  
567 [C<sub>6</sub>Py][PF<sub>6</sub>] belongs to [PF<sub>6</sub>]-based RTILs, its strong water sorption and the water clustering  
568 at high activity must be taken into account for all applications when contact with water is  
569 necessary. The present study shows how the water sorption behavior of pyridinium-based  
570 RTILs can be modulated and controlled depending on the hydration conditions.

571

## 572 **Acknowledgements**

573 The authors acknowledge the financial support provided by the Réseaux Polymères Innovants  
574 (France). This work was partially supported by the ANR project Symposium (ANR-16-CE05-  
575 0005).

576

## 577 **References**

- 578 1 S. Keskin, D. Kayrak-Talay, U. Akman, O. Hortacsu, A review of ionic liquids  
579 towards supercritical fluid applications, *J. Supercrit. Fluids* 4 (2007) 150-180.
- 580 2 J. G. Huddleston, A. E. Visser, W. M. Reichert, H. D. Willauer, G. A. Broker, R. D.  
581 Rogers, Characterization and comparison of hydrophilic and hydrophobic room  
582 temperature ionic liquids incorporating the imidazolium cation, *Green Chem.* 3 (2001)  
583 156-164.
- 584 3 J. F. Brennecke, E. J. Maginn, Ionic liquids: innovative fluids for chemical processing,  
585 *AIChE J.* 47 (2001) 2384-2389.

- 586 4 M. Freemantle, Eyes on ionic liquids. NATO workshop examines the industrial  
587 potential of green chemistry using room-temperature “designer solvents”, Chem. Eng.  
588 News 78 (2000) 37-50.
- 589 5 A.P. de los Ríos, F.J. Hernández Fernández, D. Gómez, M. Rubio, G. VÍllora,  
590 Biocatalytic transesterification of sunflower and waste cooking oils in ionic liquid  
591 media, Process Biochem.46 (2011) 1475-1480.
- 592 6 J. M. Padró, R. B. P. Vidal, M. Reta, Partition coefficients of organic compounds  
593 between water and imidazolium-, pyridinium-, and phosphonium-based ionic liquids,  
594 Anal. Bioanal. Chem.406 (2014) 8021-8031.
- 595 7 C. Zhang, C. J. Dodge, S. V. Malhotra, A. J. Francis, Bioreduction and precipitation of  
596 uranium in ionic liquid aqueous solution by *Clostridium* sp., Biores. Technol. 136  
597 (2013) 752-756.
- 598 8 D. Behar, P. Neta, C. Schultheisz, Reaction kinetics in ionic liuqids as studied by pulse  
599 radiolysis: redox reactions in the solvents methyltributylammonium  
600 bis(trifluoromethylsulfonyl)imide and *N*-butylpyridinium tetrafluoroborate, J. Phys.  
601 Chem. A 106 (2002) 3139-3147.
- 602 9 D. E. Siyutkin, A. S. Kucherenko, S. G. Zlotin, Hydroxy- $\alpha$ -amino acids modified by  
603 ionic liquid moieties: recoverable organocatalysts for asymmetric aldol reactions in the  
604 presence of water, Tetrahedron 65 (2009) 1366-1372.
- 605 10 H. Abdolmohammad-Zadeh, M. Galeh-Assadi, S. Shabkhizan, H. Mousazadeh, Sol-  
606 gel processed pyridinium ionic liquid – modified silica as a new sorbent for separation  
607 and quantification of iron in water samples, Arab. J. Chem. 9 (2016) S587-S594.
- 608 11 H. Abdolmohammad-Zadeh, G.H. Sadeghi, A novel microextraction technique based  
609 on 1-hexylpyridinium hexafluorophosphate ionic liquid for the preconcentration of  
610 zinc in water and milk samples, Anal. Chim. Acta 649 (2009) 211-217.
- 611 12 H. Abdolmohammad-Zadeh, G.H. Sadeghi, Combination of ionic liquid-based  
612 dispersive liquid-liquid micro-extraction with stopped-flow spectrofluorometry for the  
613 pre-concentration and determination of aluminum in natural waters, fruit juice and  
614 food samples, Talanta 81 (2010) 778-785.
- 615 13 M. Zeeb, M. Sadeghi, Sensitive determination of terazosin in pharmaceutical  
616 formulations and biological samples by ionic-liquid microextraction prior to  
617 spectrofluorimetry, Intern. J. Anal. Chem. 4 (2012) article ID 546282.
- 618 14 L. Cammarata, S. G. Kazarian, P. A. Salter, T. Welton, Molecular states of water in  
619 room temperature ionic liquids, Phys. Chem. Chem. Phys. 3 (2001) 5192-5200.

- 620 15 C. D. Tran, S. H. D. Lacerda, D. Oliveira, Absorption of water by room-temperature  
621 ionic liquids: effect of anions on concentration and state of water, *Appl. Spectrosc.* 57  
622 (2003) 152-157.
- 623 16 J. L. Anthony, E. J. Maginn, J. F. Brennecke, Solution thermodynamics of  
624 imidazolium-based ionic liquids and water, *J. Phys. Chem. B* 105 (2001) 10942-  
625 10949.
- 626 17 Y. Wang, H. Li, S. A. Han, A theoretical investigation of the interactions between  
627 water molecules and ionic liquids, *J. Phys. Chem. B* 110 (2006) 24646-24651.
- 628 18 K. R. Seddon, A. Stark, M. J. Torres, Influence of chloride, water, and organic  
629 solvents on the physical properties of ionic liquids, *Pure Appl. Chem.* 72 (2000) 2275-  
630 2287.
- 631 19 J. M. Andanson, F. Jutz, A. Baiker, Investigation of binary and ternary systems of  
632 ionic liquids with water and/or supercritical CO<sub>2</sub> by in situ attenuated total reflection  
633 infrared spectroscopy, *J. Phys. Chem. B* 114 (2010) 2111-2117.
- 634 20 J. S. Wilkes, M. J. Zaworotko, Air and water stable 1-ethyl-3-methylimidazolium  
635 based ionic liquids, *J. Chem. Soc., Chem. Commun.* 13 (1992) 965-967.
- 636 21 C. M. S. S. Neves, M. L. S. Batista, A. F. M. Claudio, L. M. N. B. F. Santos, I. M.  
637 Marrucho, M. G. Freire, J. A. P. Coutinho, Thermophysical properties and water  
638 saturation of [PF<sub>6</sub>]-based ionic liquids, *J. Chem. Eng. Data* 55 (2010) 5065-5073.
- 639 22 M. G. Freire, C. M. S. S. Neves, P. J. Carvalho, R. L. Gardas, A. M. Fernandes, I. M.  
640 Marrucho, L. M. N. B. F. Santos, J. A. P. Coutinho, Mutual solubilities of water and  
641 hydrophobic ionic liquids, *J. Phys. Chem. B* 111 (2007) 13082-13089.
- 642 23 X.-Z. Yang, J. Wang, G.-S. Li, Z.-Z. Zhang, Solubilities of 1-ethylpyridinium  
643 hexafluorophosphate in ethanol+water from (278.15 to 345.15) K, *J. Chem. Eng. Data*  
644 54 (2009) 75-77.
- 645 24 N. Papaiconomou, J. Salminen, J.-M. Lee, J. M. Prausnitz, Physicochemical properties  
646 of hydrophobic ionic liquids containing 1-octylpyridinium, 1-octyl-2-  
647 methylpyridinium, or 1-octyl-4-methylpyridinium cations, *J. Chem. Eng. Data* 52  
648 (2007) 833-840.
- 649 25 J. M. Padró, M. Reta, Solvatochromic parameters of imidazolium-,  
650 hydroxyammonium-, pyridinium- and phosphonium-based room temperature ionic  
651 liquids, *J. Mol. Liq.* 213 (2016) 107-114.
- 652 26 C. Chappéy, K. Fatyeyeva, E. Rynkowska, W. Kujawski, L. Karpenko-Jereb, A.-M.  
653 Kelterer, S. Marais, Sulfonic membrane sorption and permeation properties:

654 complementary approaches to select a membrane for pervaporation, *J. Phys. Chem. B*  
655 121 (2017) 8523-8538.

656 27 J. Barrie, B. Platt, The diffusion and clustering of water vapour in polymers, *Polymer*  
657 4 (1963) 303-313.

658 28 E. Favre, P. Schaetzel, Q.T. Nguyen, R. Clément, J. Néel, Sorption, diffusion and  
659 vapor permeation of various penetrants through dense poly(dimethylsiloxane)  
660 membranes: a transport analysis, *J. Membr. Sci.* 92 (1994) 169-184.

661 29 L. Perrin, Q.T. Nguyen, D. Sacco, P. Lochon, Experimental studies and modelling of  
662 sorption and diffusion of water and alcohols in cellulose acetate, *Polym. Int.* 42 (1997)  
663 9-16.

664 30 B.H. Zimm, J.L. Lundberg, Sorption of vapors by high polymers, *J. Phys. Chem.* 60  
665 (1956) 425-428.

666 31 J.L. Lundberg, Molecular clustering and segregation in sorption systems, *Pure Appl.*  
667 *Chem.* 31 (1972) 261-282.

668 32 H.W. Starkweather, Clustering of water in polymers, *Polym. Lett.* 1 (1963) 133-138.

669 33 P. Aranda, W.J. Chen, C.R. Martin, Water transport across  
670 polystyrenesulfonate/alumina composite membranes, *J. Membr. Sci.* 99 (1995) 185-  
671 195.

672 34 M.A. Del Nobile, G. Mensitieri, A. Sommazzi, Gas and water vapour transport in a  
673 polyketone terpolymer, *Polymer* 36 (1995) 4943-4950.

674 35 A. M. O'Mahony, D. S. Silvester, L. Aldous, C. Hardacre, R. G. Compton, Effect of  
675 water on the electrochemical window and potential limits of room-temperature ionic  
676 liquids, *J. Chem. Eng. Data* 53 (2008) 2884-2891.

677 36 M.D. Bermejo, T.M. Fieback, A. Martin, Solubility of gases in 1-alkyl-3-  
678 methylimidazolium alkyl sulfate ionic liquids: experimental determination and  
679 modelling, *J. Chem. Thermodyn.* 58 (2013) 237-244.

680 37 X. Liu, W. Afzal, G. Yu, M. He, J.M. Prausnitz, High solubilities of small  
681 hydrocarbons in trihexyl tetradecylphosphonium bis(2,4,4-trimethylpentyl)  
682 phosphinate, *J. Phys. Chem. B* 113 (2013) 10534-10539.

683 38 M.B. Shiflett, D.R. Corbin, B.A. Elliott, A. Yokozeki, Sorption of trifluoromethane in  
684 zeolites and ionic liquid, *J. Chem. Thermodyn.* 64 (2013) 40-49.

685 39 D. Camper, J. Bara, C. Koval, R. Noble, Bulk-fluid solubility and membrane  
686 feasibility of Rmim-based room-temperature ionic liquids, *Ind. Eng. Chem. Res.* 45  
687 (2006) 6279-6283.

688 40 A.-L. Revelli, F. Mutelet, J.-N. Jaubert, (Vapor+liquid) equilibria of binary mixtures  
689 containing light alcohols and ionic liquids, *J. Chem. Thermodyn.* 42 (2010) 177-181.

690 41 H. Feng, Modeling of vapor sorption in glassy polymers using a new dual mode  
691 sorption model based on multilayer sorption theory, *Polymer* 48 (2007) 2988-3002.

692 42 Y. Li, Q.T. Nguyen, K. Fatyeyeva, S. Marais, Water sorption behavior in different  
693 aromatic ionomer composites analyzed with a “new dual-mode sorption” model,  
694 *Macromolecules* 47 (2014) 6331-6342.

695 43 E. Zhao, M. Yu, R.E. Sauvé, M.K. Khoshkbarchi, Extension of the Wilson model to  
696 electrolyte solutions, *Fluid Phase Equilib.* 173 (2000) 161-175.

697 44 J.A. Lazzus, J. Martin, Activity coefficient models to describe isothermal vapor-liquid  
698 equilibrium of binary systems containing ionic liquids, *J. Eng; Thermophys.* 19 (2010)  
699 170-183.

700 45 M. Kahrizi, N. Kasiri, T. Mohammadi, S. Zhao, Introducing sorption coefficient  
701 through extended UNIQUAC and Flory-Huggins models for improved flux prediction  
702 in forward osmosis, *Chem. Eng. Sci.* 198 (2019) 33-42.

703 46 H. Kuramochi, K. Maeda, S. Kato, M. Osako, K. Nakamura, S.-i. Sakai, Application  
704 of UNIFAC models for prediction of vapor-liquid and liquid-liquid equilibria relevant  
705 to separation and purification processes of crude biodiesel fuel, *Fuel* 88 (2009) 1472-  
706 1477.

707 47 E.O. Timmermann, J. Chirife, H.A. Iglesias, Water sorption isotherms of foods and  
708 foodstuffs: BET or GAB parameters? *J. Food Eng.* 48 (2001) 19-31.

709 48 D.J. Sampson, Y.K. Chang, H.P. Vasantha Rupasinghe, Q. UZ Zaman, A dual-view  
710 computer-vision system for volume and image texture analysis in multiple apple slices  
711 drying, *J. Food Eng.* 127 (2014) 49-57.

712 49 V. Klika, J. Kubant, M. Pavelka, J.B. Benziger, Non-equilibrium thermodynamic  
713 model of water sorption in Nafion membranes, *J. Membr. Sci.* 540 (2017) 35-49.

714 50 C. Mericer, M. Minelli, M.G. Baschetti, T. Lindstrom, Water sorption in  
715 microfibrillated cellulose (MFC): the effect of temperature and pretreatment,  
716 *Carbohydr. Polym.* 174 (2017) 1201-1212.

717 51 K. Fatyeyeva, S. Rogalsky, O. Tarasyuk, C. Chappey, S. Marais, Vapour sorption and  
718 permeation behaviour of supported ionic liquid membranes: application for organic  
719 solvent/water separation, *React. Function. Polym.* 130 (2018) 16-28.

720 52 H. Zhu, R. Vijayaraghavan, D. R. MacFarlane, M. Forsyth, Self-assembled structure  
721 and dynamics of imidazolium-based protic salts in water solution, *Phys. Chem. Chem.*  
722 *Phys.* 21 (2019) 2691-2696.

723 53 A. Maiti, A. Kumar, R. D. Rogers, Water-clustering in hygroscopic ionic liquids -an  
724 implicit solvent analysis, *Phys. Chem. Chem. Phys.* 14 (2012) 5139-5146.

725 54 C. G. Hanke, R. M. Lynden-Bell, A simulation study of water - dialkylimidazolium  
726 ionic liquid mixtures, *J. Phys. Chem. B* 107 (2003) 10873-10878.

727 55 T. Singh, A. Kumar, Cation-anion-water interactions in aqueous mixtures of  
728 imidazolium based ionic liquids, *Vib. Spectrosc.* 55 (2011) 119-125.

729 56 M. Moreno, F. Castiglione, A. Mele, C. Pasqui, G. Raos, Interaction of water with the  
730 model ionic liquid [bmim][BF<sub>4</sub>]: molecular dynamics simulations and comparison  
731 with NMR data, *J. Phys. Chem. B* 112 (2008) 7826-7836.

732 57 A. Dahi, K. Fatyeyeva, C. Chappey, D. Langevin, S. P. Rogalsky, O. P. Tarasyuk, S.  
733 Marais, Water sorption properties of room-temperature ionic liquids ver the whole  
734 range of water activity and molecular states of water in these media, *RSC Adv.* 5  
735 (2015) 76927-76938.

736 58 N.-N. Wang, Q.-G. Zhang, F.-G. Wu, Q.-Z. Li, Z.-W. Yu, Hydrogen bonding  
737 interactions between a representative pyridinium-based ionic liquid [BuPy][BF<sub>4</sub>] and  
738 water/dimethyl sulfoxide, *J. Phys. Chem. B* 114 (2010) 8689-8700.

739 59 S. Marais, Q. T. Nguyen, D. Langevin, M. Métayer, Transport of water and gases  
740 through EVA copolymer films, EVA<sub>70</sub>/PVC, and EVA<sub>70</sub>/PVC/gluten blends,  
741 *Macromol. Symp.* 175 (2001) 329-347.

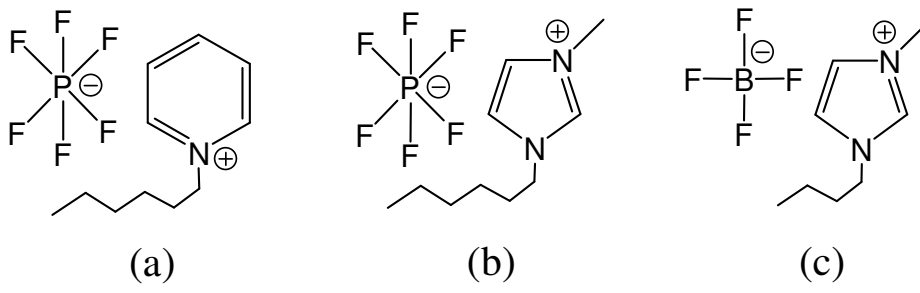
742 60 K. Popov, H. Rönkkömäki, M. Hannu-Kuure, T. Kuokkanen, M. Lajunen, A. Vendilo,  
743 P. Oksman, L. H. J. Lajunen, Stability of crown-ether complexes with alkali-metal  
744 ions in ionic liquid-water mixed solvents, *J. Incl. Phenom. Macrocycl. Chem.* 59  
745 (2007) 377-381.

746 61 L. Wang, H. Sun, G. Zhang, S. Sun, X. Fu, Heavy metal pollution of the world largest  
747 antimony mine-affected agricultural soils in Hunan province (China), *J. Soils*  
748 *Sediments* 13 (2013) 450-456.

749 62 J. de Riva, V.R. Ferro, D. Moreno, I. Diaz, J. Palomar, Aspen Plus supported  
750 conceptual design of the aromatic-aliphatic separation from low aromatic content  
751 naphtha using 4-methyl-N-butylpyridinium tetrafluoroborate ionic liquid, *Fuel Proces.*  
752 *Technol.* 146 (2016) 29-38.



- 753 63 R. Fortunato, C. A. M. Afonso, M. A. M. Reis, J. G. Crespo, Supported liquid  
754 membranes using ionic liquids: study of stability and transport mechanisms, *J. Membr.*  
755 *Sci.* 242 (2004) 197-209.
- 756 64 R. Fortunato, M. J. Gonzalez-Munoz, M. Kubasiewicz, S. Luque, J. R. Alvarez, C. A.  
757 M. Afonso, I. M. Coelho, J. G. Crespo, Liquid membranes using ionic liquids: the  
758 influence of water on solute transport, *J. Membr. Sci.* 249 (2005) 153-162.
- 759 65 P. Scovazzo, Testing and evaluation of room temperature ionic liquid (RTIL)  
760 membranes for gas dehumidification, *J. Membr. Sci.* 355 (2010) 7-17.
- 761 66 E. Zoidis, J. Yarwood, T. Tassaing, Y. Danten, M. Besnard, Vibrational spectroscopic  
762 studies on the state of aggregation of water in carbon tetrachloride, in dioxane and in  
763 the mixed solvents, *J. Mol. Liq.* 64 (1995) 197-210.
- 764 67 H. Kusanagi, S. Yukawa, Fourier transform infra-red spectroscopic studies of water  
765 molecules sorbed in solid polymers, *Polymer* 35 (1994) 5637-5640.
- 766 68 Y. Danten, M. I. Cabaco, M. Besnard, Interaction of water diluted in 1-butyl-3-methyl  
767 imidazolium ionic liquids by vibrational spectroscopy modeling, *J. Mol. Liq.* 153  
768 (2010) 57-66.
- 769 69 P. A. Bergstrom, J. Lindgren, O. Kristiansson, An IR study of the hydration of  $\text{ClO}_4^-$ ,  
770  $\text{NO}_3^-$ ,  $\text{I}^-$ ,  $\text{Br}^-$ ,  $\text{Cl}^-$ , and  $\text{SO}_4^{2-}$  anions in aqueous solution, *J. Phys. Chem.* 95 (1991)  
771 8575-8580.



4

5

6

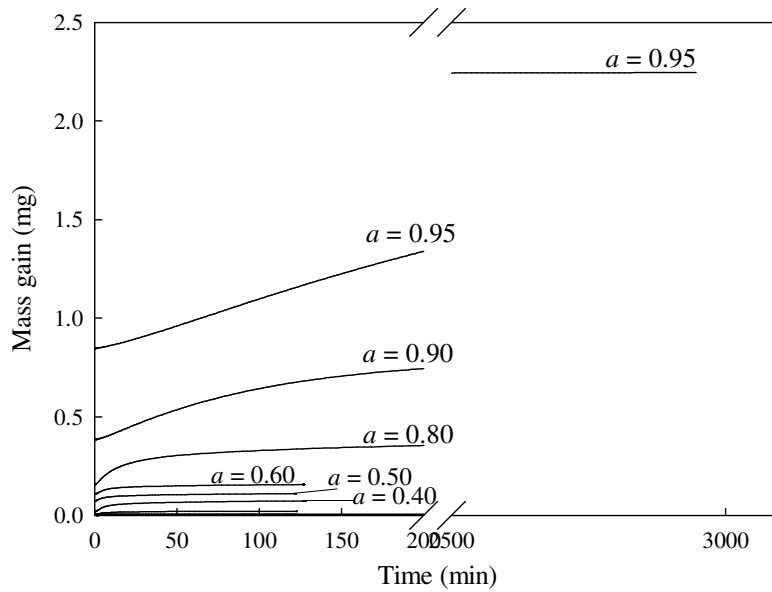
7

8

9

10

**Fig. 1.** Chemical structure of (a) [C6Py][PF6], (b) [C6C1im][PF6], and (c) [C4C1im][BF4].



11

12

**Fig. 2.** Water vapor sorption kinetics of [C6Py][PF6] at different water activity values.

13

14

15

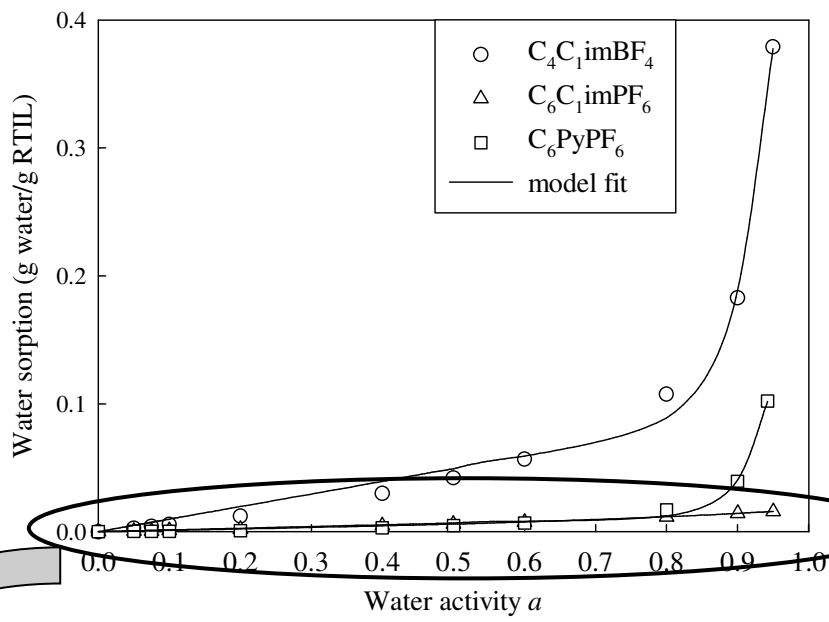
16

17

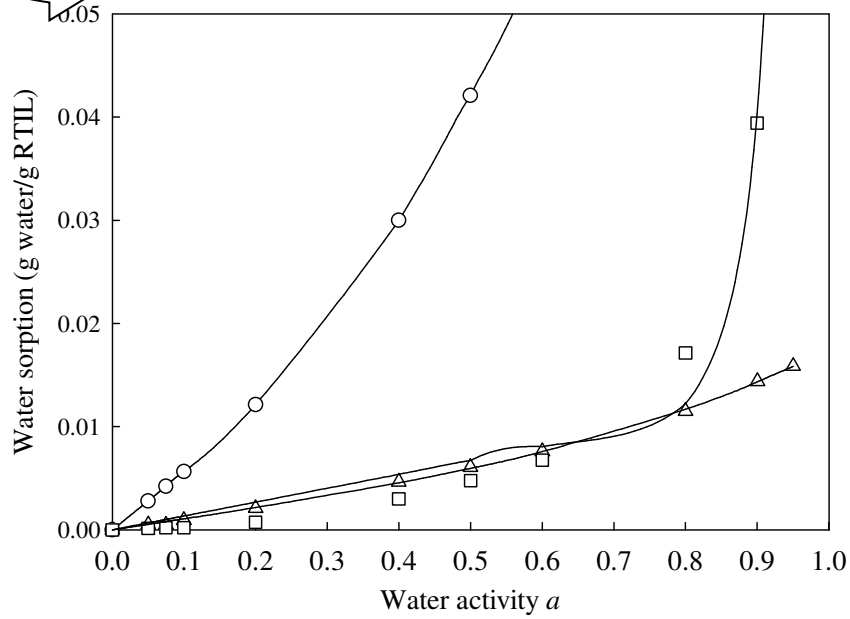
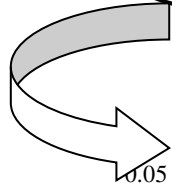
18

19

20



21



29

30 **Fig. 3.** Water vapor sorption isotherms of different RTILs. Solid lines are the fit according to  
31 the Henry-clustering model (Eq. 2).

32

33

34

35

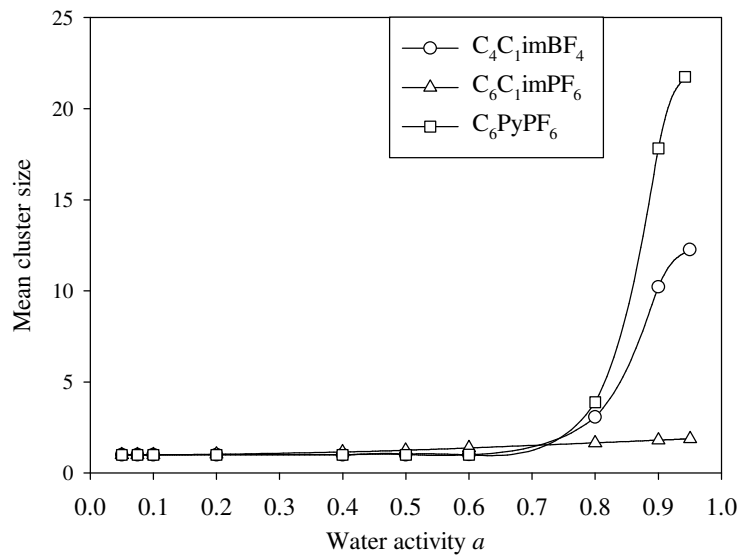
36

37

38

39

40



41 **Fig. 4.** Mean cluster size of  $[C_6Py][PF_6]$ ,  $[C_6C_1im][PF_6]$  and  $[C_4C_1im][BF_4]$  as a function of  
42 water activity.

43

44

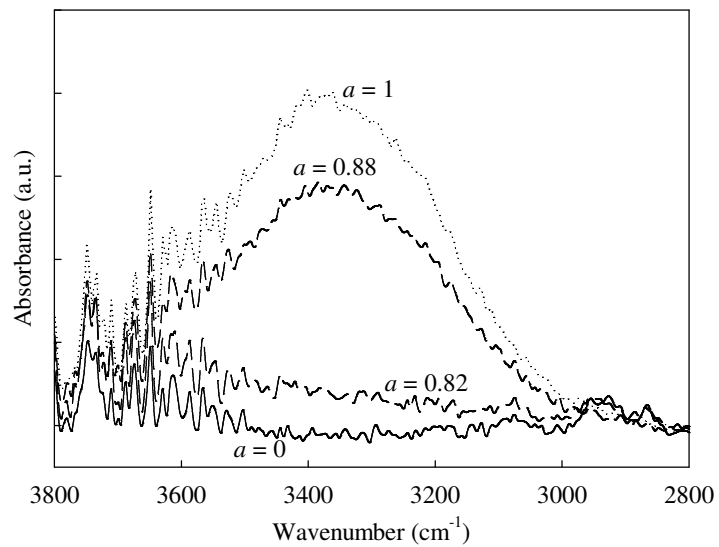
45

46

47

48

49



50

51 **Fig. 5.** ATR-IR spectra of  $[C_6Py][PF_6]$  as a function of water activity  $a$ .

52

**Table 1.** Parameters of the Henry-clustering model (Eq. 2).

RTIL	Parameter			Ref.
	$k_D$ (g water/g RTIL)	$K_a$ ((g water/g RTIL) <sup>1-n</sup> )	$n$	
[C <sub>6</sub> Py][PF <sub>6</sub> ]	$1.3 \cdot 10^{-2}$	$1.4 \cdot 10^{45}$	25.1	This work
[C <sub>6</sub> C <sub>1</sub> im][PF <sub>6</sub> ]	$1.1 \cdot 10^{-2}$	$1.2 \cdot 10^4$	3.5	<sup>36</sup>
[C <sub>4</sub> C <sub>1</sub> im][BF <sub>4</sub> ]	$9.8 \cdot 10^{-2}$	$1.2 \cdot 10^{18}$	19.3	<sup>36</sup>